Electronic Supplementary Material (ESI) for ChemComm.

Supplementary information for Ni-modified β-FeOOH nanorod cocatalysts for oxygen evolution utilising photoexcited holes on N2p level in N-doped TiO_2 electrode

Takahiro Ikeda, Tomiko M. Suzuki, Takeo Arai and Takeshi Morikawa

Preparation of N-TiO_2 photoanode

In the vacuum chamber of a high-frequency magnetron sputtering system (< 5×10^{-5} Pa), an indium tin oxide (ITO)-coated glass substrate (Geomatec, 2.1 cm × 2.1 cm) covered with a layer of SnO_2 and a TiO_2 target (High Purity Chemical, 99.99%, φ102 mm) were placed opposite each other. After introducing the Ar/O_2 gas mixture (10/40 sccm), 200 W of electric power was applied to the TiO_2 target to form a plasma; the power intensity then the power was then increased to 600 W and held for more than 20 min (pre-sputtering). The gas composition was gradually changed to Ar/N_2 (30/20 sccm) over approximately 1 min so as not to extinguish the plasma and then maintained until the pressure became stable. The shutter was then opened, and N-TiO_2 films were formed for approximately 45 min. The obtained electrodes were annealed at 550 °C for 2 h under a N_2 atmosphere to obtain N-TiO_2 photoanodes.

Synthesis of Ni-modified β-FeOOH and β-FeOOH nanorods colloidal solution[S1]

A colloidal solution of Ni-modified β-FeOOH nanorods (FeNi NRs; diameters of 3 nm and lengths of 13 nm) was synthesised by adding $Ni(NO_3)_2\cdot6H_2O$ and ethylenediamine to 500 mL of 0.1 M $FeCl_3\cdot6H_2O$ aqueous solution, adjusting the pH range to 2.0–2.4, stirring for 30 min at room temperature, and then allowing the solution to stand overnight.[S1] As a result, a colloidal solution of FeNi NRs was obtained. A colloidal solution of β-FeOOH nanorods (Fe NRs; diameters of 3 nm and lengths of 13 nm) was synthesised using the same procedure as described above without the addition of Ni salt.

Loading of $Ni(OH)_2$-coated β-FeOOH:Ni and Fe NRs on a N-TiO_2 photoanode

Using a spin coater (Mikasa, MS-A100), 100 μL of FeNi NR and β-FeOOH nanorod (Fe NR) colloidal aqueous solutions were dropped onto the N-TiO_2 photoanodes, and spin-coated at 1000 rpm for 10 s. Then, the photoanodes were heated at 60 °C for approximately 10 min to dry. FeNi NRs in the colloidal solution become amorphous $Ni(OH)_2$-coated β-FeOOH:Ni nanorods (Ni/Fe ratio ≈ 15 at%) after drying, followed by immersion in the electrolyte. The N-TiO_2 photoanodes loaded with FeNi NRs and Fe NRs are referred to as FeNi/N-TiO_2 and Fe/N-TiO_2, respectively.

Characterisation

The X-ray diffraction (XRD) patterns were taken for bare N-TiO_2 before and after annealing, Fe/N-TiO_2 and FeNi/N-TiO_2 (Rigaku, Ultima IV, CuKα). The compositions of FeNi/N-TiO_2 and Fe/N-TiO_2 were analysed by inductive coupled plasma mass spectroscopy (ICP-MS, Agilent Technologies, Agilent 8900). The chemical states and concentrations of Ni and Fe were determined by X-ray photoelectron spectroscopy (XPS, Quantera SXM, ULVAC-PHI) using monochromated Al Kα radiation. All spectra were corrected relative to the C 1s peak at 285 eV. The chemical states of Fe and Ni were evaluated by X-ray absorption fine structure (XAFS) spectroscopy. Fe and Ni K-edge X-ray absorption near edge structure (XANES) data were acquired in the transmission mode using the BL33XU beamline at SPring-8 (Hyogo, Japan). The height differences between the ITO top surface and the N-TiO_2 top surface were measured using a step meter (Bruker, Dektak3) at 10 different points on the fabricated N-TiO_2 photoanodes before annealing. The average value was used as the thickness of the sputtered N-TiO_2 film. The top surface and the cross-section of the fabricated FeNi/N-TiO_2 were observed by SEM (HITACHI, S-4800) at 5.0 kV and 30,000–200,000× magnification. Cross-sectional images were obtained after resin filling, ion milling, and Pt sputter coating.

Photoelectrochemical measurements

Photoelectrochemical measurements were performed using a potentiostat (ALS, CHI614C) in a three-electrode configuration consisting of a sample electrode with an area of approximately 4 cm^2 as the working electrode, a Pt wire as the counter electrode, and an Ag/AgCl electrode as the reference electrode (+0.199 V vs. NHE). The measurements were performed at room temperature in air using a 1 M KOH aqueous solution (pH 14 vs. RHE) as the electrolyte. Light from a 300 W Xe lamp (Asahi Spectroscopy, MAX-303) through a cutoff filter ($\lambda > 420$ nm) was irradiated from the back of the sample electrode (ITO glass side) during the measurements. For the TiO_2 electrode, the light source was a solar simulator without cutoff filters.

The wavelength dependence of the photocurrent was investigated by irradiating monochromatised light with the corresponding bandpass filter applying 0 V vs. Ag/AgCl (1.03 V vs. RHE). The intensity of light at each wavelength was measured with an optical power meter (Hamamatsu Photonics, C9536-01 and ADCMT, 82324 B) and converted

to incident photon to current efficiency (IPCE) using the following formula:

$$\text{IPCE}\ (\%) = 1239.8 \times J\ (\text{mA}) / (\ S\ (\text{cm}^2) \times I\ (\text{mW}\cdot\text{cm}^{-2}) \times \lambda\ (\text{nm})\ ) \times 100$$

Here, J is the photocurrent generated by the light irradiation, S is the electrode area, I is the light intensity per unit area of the irradiated light, and λ is the wavelength of the irradiated light. The light intensities used for calculating IPCE are listed in Table S1.

Table S1 Light intensities at each wavelength used for calculating IPCE. The bold values were calculated by the light intensity ratio at 400 nm measured by two power meters and used for IPCE calculation.

Wavelength (nm)	light intensity by UV power meter (mW/cm^2)	light intensity by vis. power meter (mW/cm^2)	**corrected light intensity (mW/cm^2)**
340	0.912		**0.706**
360	1.05		**0.813**
380	0.936		**0.724**
400	1.07	0.828	**0.828**
420		1.179	**1.179**
440		1.359	**1.359**
460		1.826	**1.826**
480		1.856	**1.856**
500		1.655	**1.655**
520		1.956	**1.956**
540		1.771	**1.771**
560		1.674	**1.674**
580		1.900	**1.900**

The amounts of oxygen and hydrogen produced during the photoelectrochemical reaction were quantified as follows: argon bubbling was performed in a closed cell for about 1 h, followed by the constant potential measurement (0.17 V vs. Ag/AgCl (1.20 V vs. RHE)) using the above-mentioned setup, and the amount of oxygen and hydrogen produced after 2, 4, and 6 h of light irradiation was measured by using a gas chromatography system coupled with a thermal conductivity detector (Shimadzu Corporation, GC-2014).

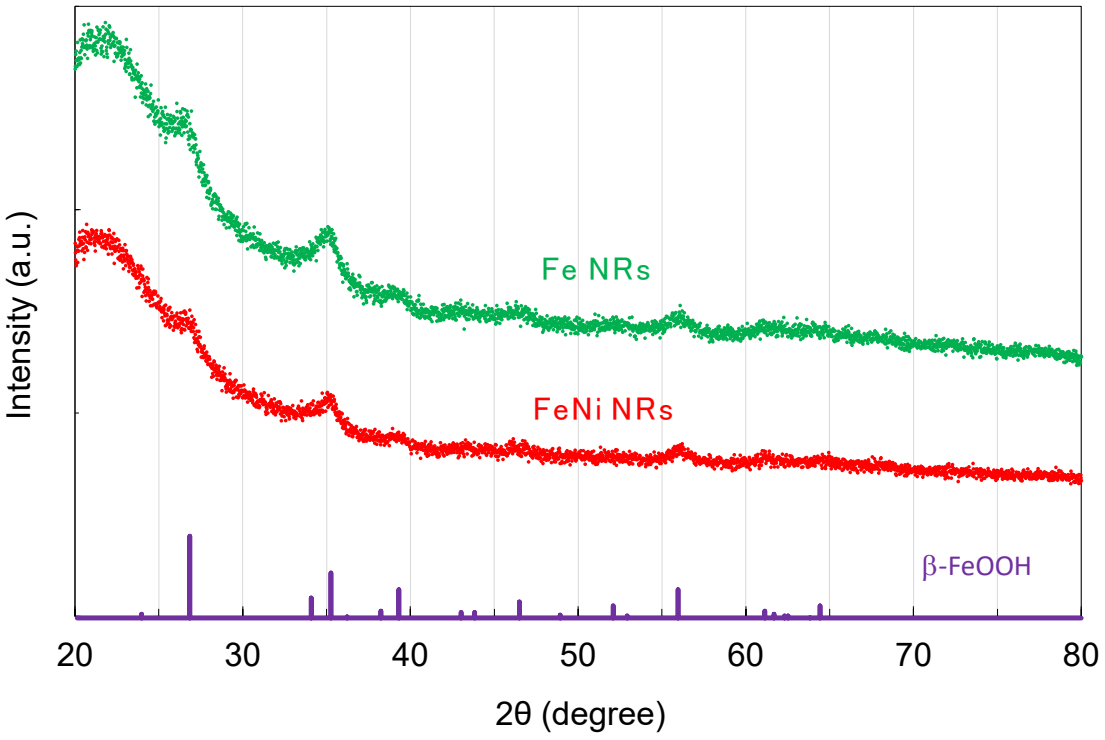

Fig. S1 XRD patterns of Fe NRs and FeNi NRs on silica filters.

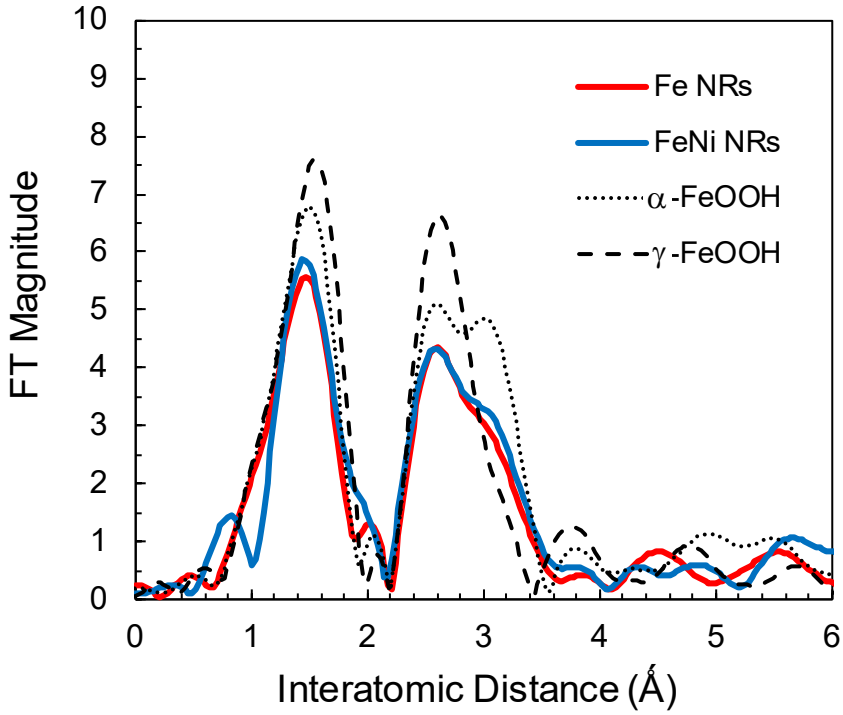

Fig. S2 k^3-weighted FT-EXAFS Fe K-edge spectra of Fe NRs and FeNi NRs on carbon papers.

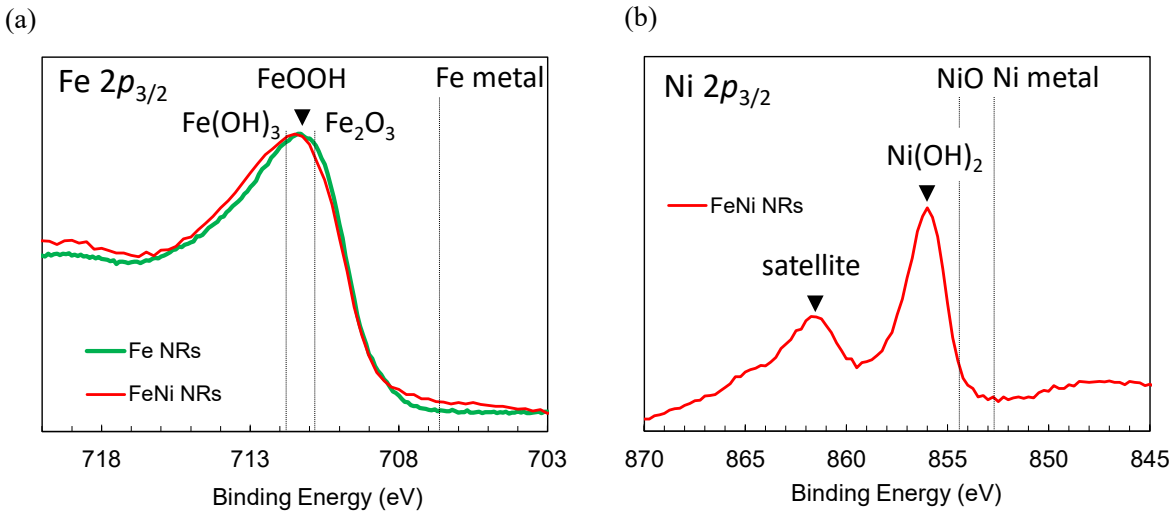

Fig. S3 (a) Fe $2p_{3/2}$ spectra for Fe NRs and FeNi NRs on carbon papers and (b) Ni $2p_{3/2}$ XPS spectrum for FeNi NRs on carbon paper. See references for peak assignment [S2-S5].

According to the reference S2 and S3, the main peaks in the range of 711.2-711.9 eV in the Fe $2p_{3/2}$ spectra and at 855.9 eV in the Ni $2p_{3/2}$ spectrum can be assigned to FeOOH and $Ni(OH)_2$, respectively. The identification of these compounds was determined including XRD and XAFS results as shown in Figs. S1, S2 and S4.

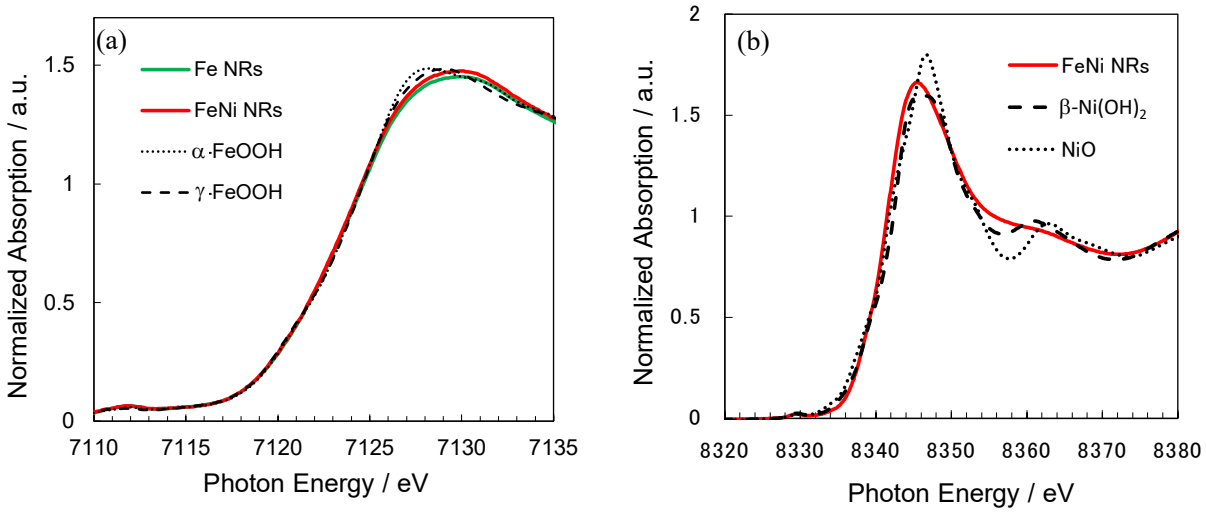

Fig. S4 XANES (a) Fe K-edge and (b) Ni K-edge spectra of FeNi NRs/carbon paper and reference samples.

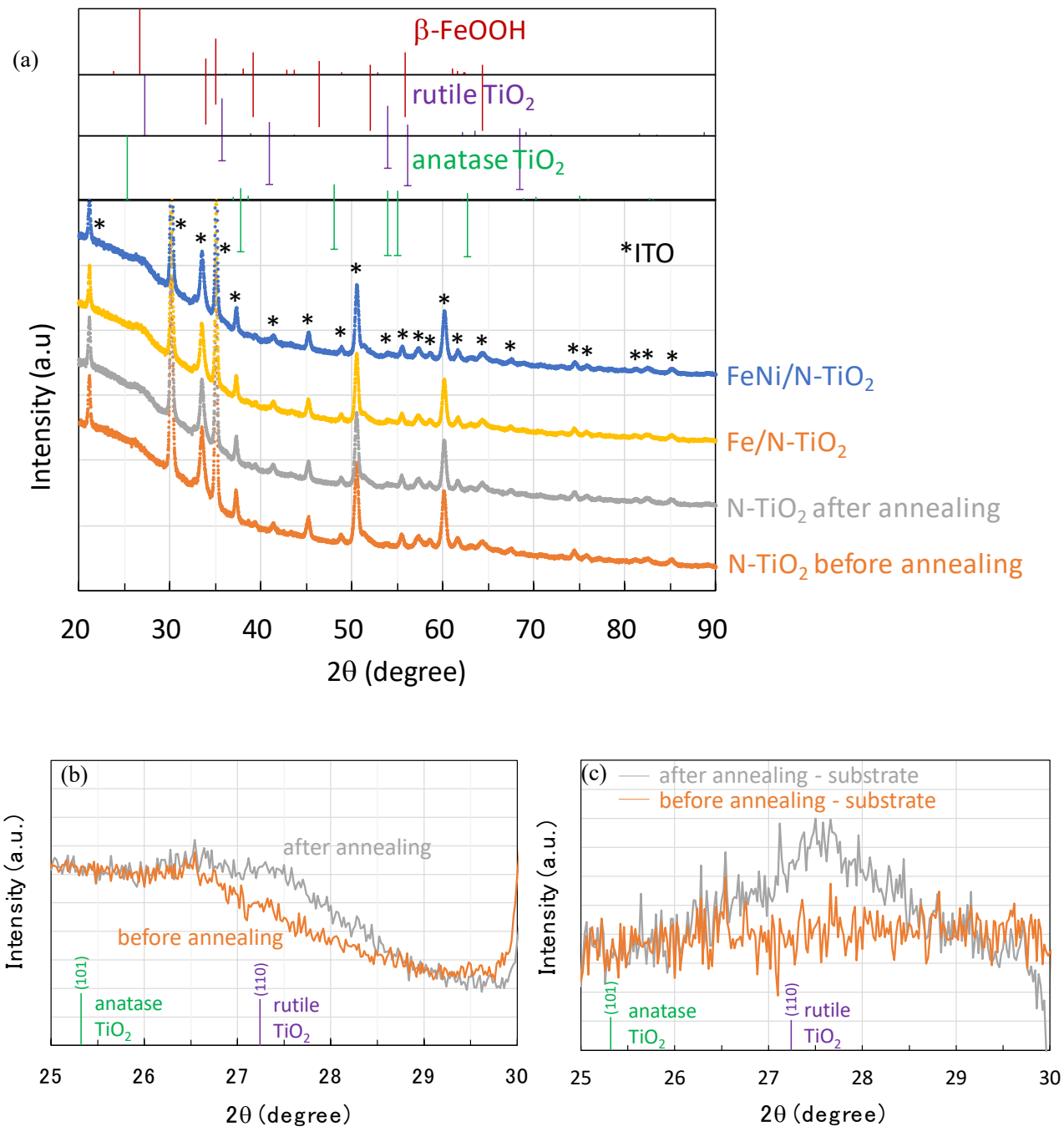

Fig. S5 (a) XRD patterns of N-TiO_2 photoanode before and after annealing, Fe/N-TiO_2 and FeNi/N-TiO_2. (b) Magnified XRD patterns of N-TiO_2 photoanode before and after annealing. (c) XRD patterns of N-TiO_2 photoanodes before and after annealing. Both patterns are the subtraction of that of the ITO/glass substrate.

In Fig. S5c, no peaks are observed before annealing, whereas clear peak appeared after annealing which is closer to (110) of rutile TiO_2 than to (101) of anatase TiO_2. This result shows the existence of rutile phase, not anatase phase, indicating amorphous N-TiO_2 crystallised to rutile phase after annealing.

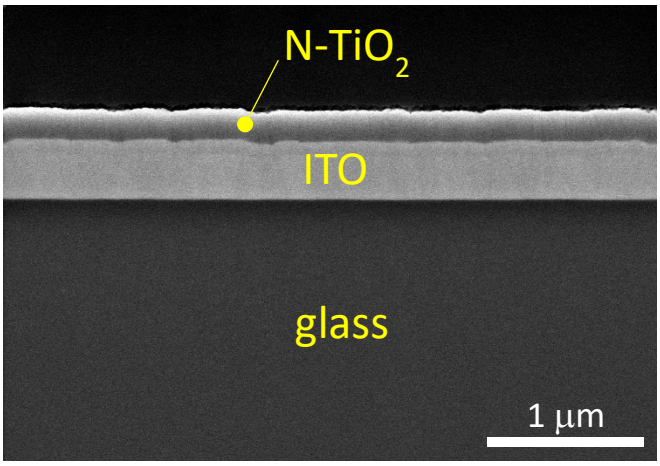

Fig. S6 Cross-sectional SEM image of a bare N-TiO_2 electrode.

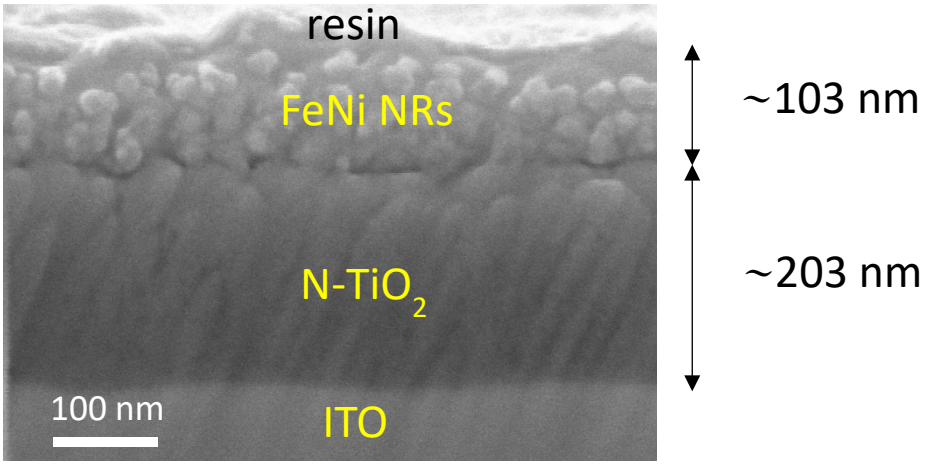

Fig. S7 High-magnification cross-sectional SEM image of FeNi/N-TiO_2.

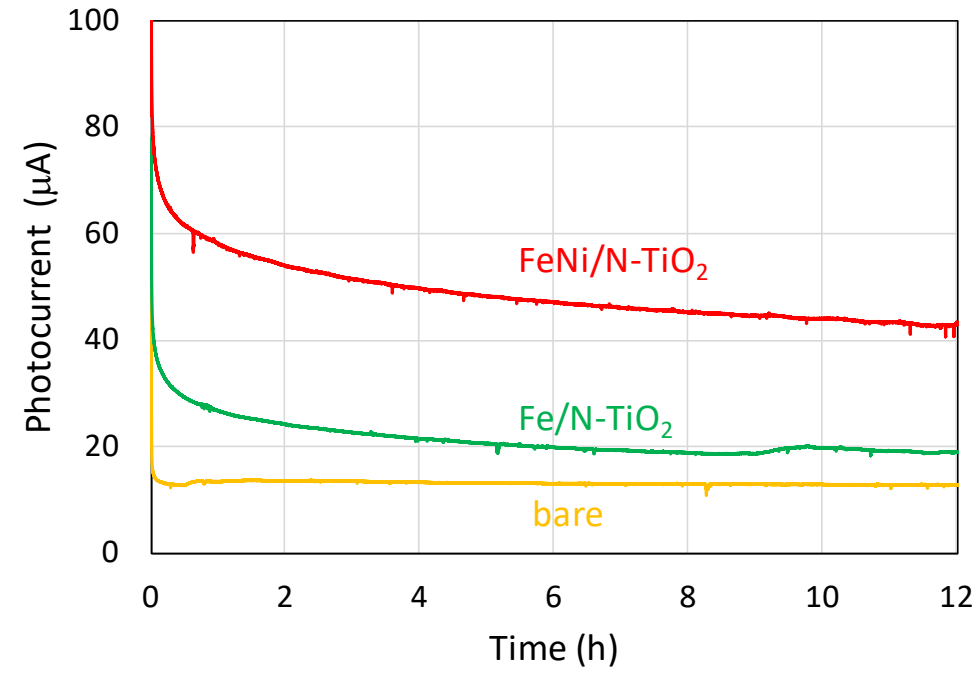

Fig. S8 Changes in photocurrents of the fabricated photoanodes over time with an applied potential of 1.03 V vs. RHE in 1 M KOH.

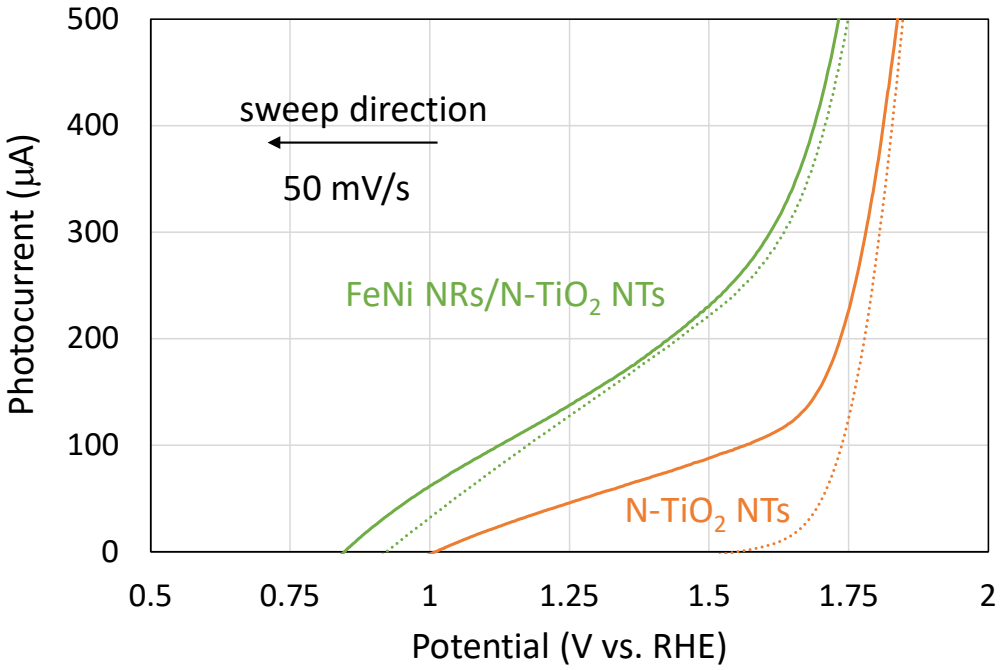

Fig. S9 Current-voltage curves of bare N-TiO_2 nanotubes (NTs) and FeNi NRs/N-TiO_2 NT electrodes under dark (dotted line) and visible-light irradiation (solid line) conditions in 1 M KOH.

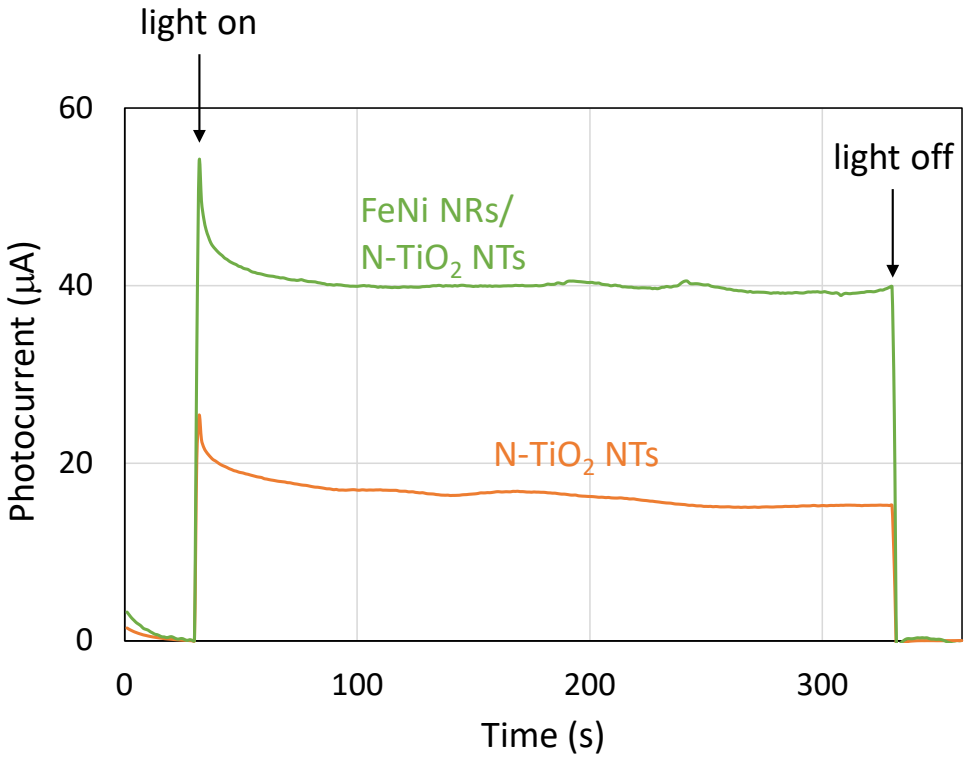

Fig. S10 Changes in photocurrents of bare N-TiO_2 NTs and FeNi NRs/N-TiO_2 NTs electrodes over time with an applied potential of 0.73 V vs. RHE in 1 M KOH.

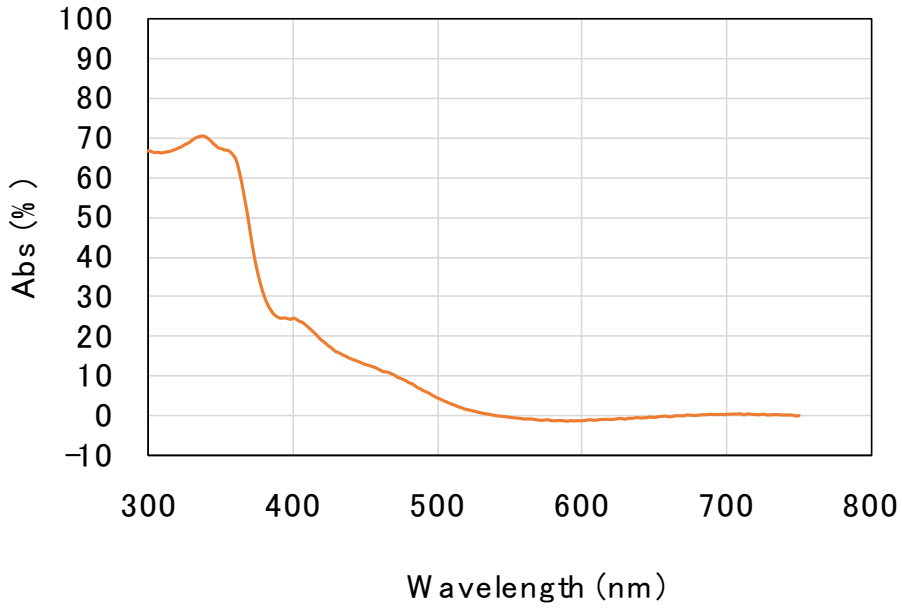

Fig. S11 UV-Vis absorption spectrum of N-TiO_2 (260 nm)/SiO_2 electrode. The preparation method is as same as N-TiO_2 electrode used in this report.

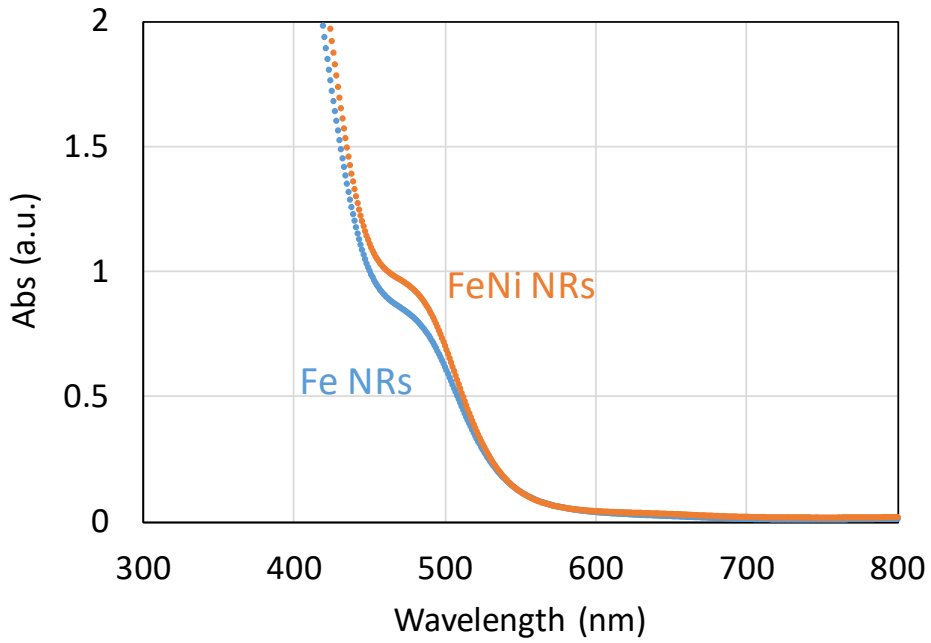

Fig. S12 UV-Vis absorption spectra of Fe NRs and FeNi NRs aqueous solution.

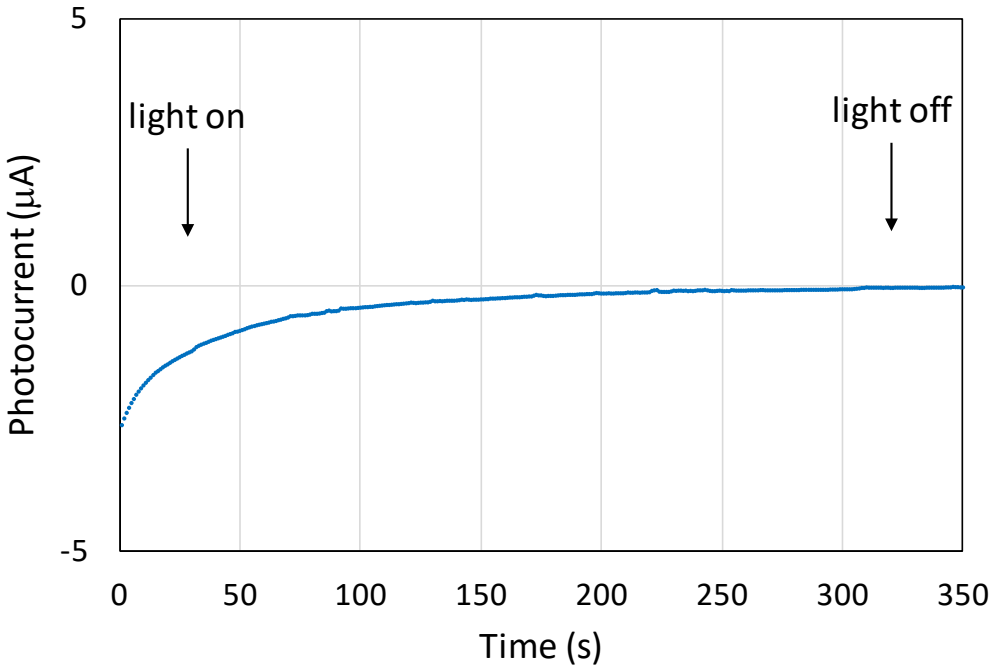

Fig. S13 Change in photocurrent of FeNi-NR-loaded ITO/glass electrode over time with an applied potential of 0.73 V vs. RHE in 1 M KOH.

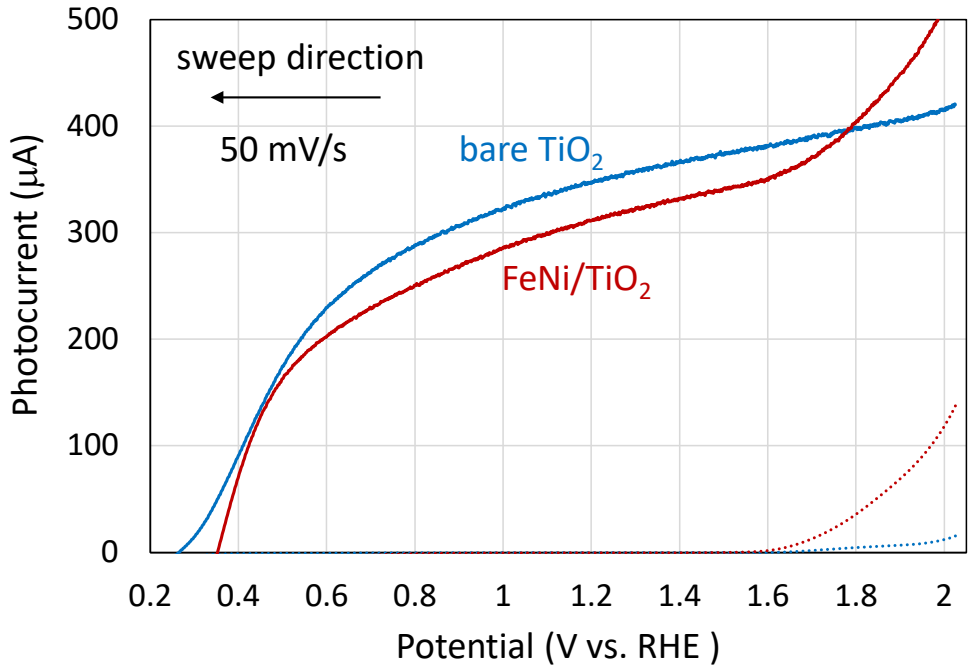

Fig. S14 Current-voltage curves of $FeNi/TiO_2$ and bare TiO_2 electrodes under dark (dotted line) and 1 sun illumination (solid line) conditions.

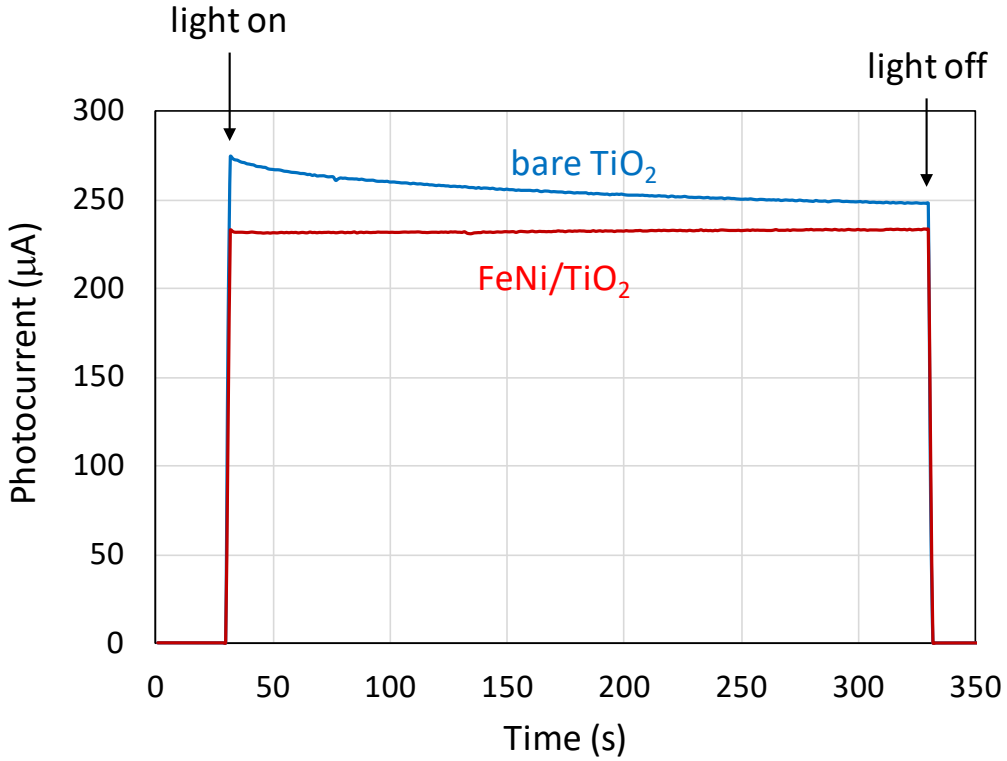

Fig. S15 Changes in photocurrents of $FeNi/TiO_2$ and bare TiO_2 electrodes over time with applied potential of 0.73 V vs. RHE under 1 sun illumination.

References

S1 T. M. Suzuki, T. Nonaka, K. Kitazumi, N. Takahashi, S. Kosaka, Y. Matsuoka, K. Sekizawa, A. Suda and T. Morikawa, *Bull. Chem. Soc. Jpn.*, 2018, **91**, 778.

S2 J. Chastain, R. C. King, Jr., Handbook of X-ray Photoelectron Spectroscopy p.81, Physical Electronics, Inc., USA, 1992.

S3 D. Briggs, M. P. Seah, Practical surface analysis second edition Vol. 1, p.608, Wiley, UK, 1990.

S4 D. Zhu, C. Guo, J. Liu, L. Wang, Y. Du and S.-Z. Qiao, *Chem. Commun.*, 2017, **53**, 10906.

S5 A. N. Mansour, *Surface Science Spectra* 1994, **3**, 239.